Title: Agricultural drought monitoring with Sentinel-1 Cross-Ratio in heterogeneous tropical agriculture: a Mozambique case study

Authors and Affiliations:

- Carina Villegas-Lituma[a] — carina.villegas@tuwien.ac.at
- Mariette Vreugdenhil[a]
- Samuel Massart[b]
- Ignacio Borlaf-Menal[a]
- Bernhard Raml[a]
- Rafael Rogério Borguete[c]
- Wolfgang Wagner[a]

[a]Department of Geodesy and Geoinformation, Vienna University of Technology, Wiedner Hauptstrasse 8, 1040 Vienna, Austria
[b]Earth and Life Institute, Catholic University of Louvain, Croix du Sud 2, 1348 Ottignies-Louvain-la-Neuve, Belgium
[c]Department of Rural Engineering, Faculty of Agronomy and Forestry Engineering, University Eduardo Mondlane, Av. Julius Nyerere, 3453 Maputo, Mozambique

Preprint Status Statement:

This manuscript is a non-peer-reviewed preprint submitted to EarthArXiv. It has also been submitted to the *International Journal of Remote Sensing* (IJRS) for peer review and is currently under review.

RESEARCH PAPER

Agricultural drought monitoring with Sentinel-1 Cross-Ratio in heterogeneous tropical agriculture: a Mozambique case study

Carina Villegas-Lituma[a], Mariette Vreugdenhil[a], Samuel Massart[b], Ignacio Borlaf-Menal[a], Bernhard Raml[a], Rafael Rogério Borguete[c] and Wolfgang Wagner[a]

[a]Department of Geodesy and Geoinformation, Vienna University of Technology, Wiedner Hauptstrasse 8, 1040 Vienna, Austria; [b]Earth and Life Institute, Catholic University of Louvain, Croix du Sud 2, 1348 Ottignies-Louvain-la-Neuve, Belgium; [c] Department of Rural Engineering, Faculty of Agronomy and Forestry Engineering, University Eduardo Mondlane, Av. Julius Nyerere, 3453 Maputo, Mozambique

ABSTRACT

Agricultural drought monitoring is essential for food security in tropical regions where rain-fed agriculture predominates. Operational early warning systems rely primarily on optical vegetation indices, but cloud cover limits their usability during critical growing periods. SAR satellites can observe through clouds, yet their adoption in agricultural drought monitoring remains limited. This study evaluates Sentinel-1 CR, a SAR-based vegetation indicator sensitive to crop water content and canopy structure, for drought monitoring across six districts in central and southern Mozambique. Using data from 2019 to 2024, we track drought propagation from precipitation (CHIRPS) through soil moisture (ASCAT) to vegetation response (CR and NDVI). Results show that CR correlates positively with NDVI over cropland, and that vegetation response corresponds more closely with soil moisture than with precipitation across most land cover types, though shrubland shows stronger precipitation dependence, indicating land-cover-specific pathways. CR captured the 2019/2020 El Niño drought and subsequent recovery across all districts. However, CR interpretation depends on land cover composition: cropland-dominated areas show clear seasonal patterns enabling anomaly-based drought detection, while heterogeneous cropland-forest/shrub mosaics typical of rain-fed systems require land cover stratified analysis at high resolution to isolate cropland-specific responses. These findings demonstrate that SAR-based vegetation monitoring can complement optical approaches for drought early warning in cloud-prone tropical regions.

KEYWORDS

Sentinel-1, Cross Ratio, NDVI, dense vegetation, rain-fed systems, agricultural drought

Abbreviations: AppEEARS, Application for Extracting and Exploring Analysis Ready Samples; ASCAT, Advanced SCATterometer; CCI, Climate Change Initiative; CDR, Climate Data Record; CHIRPS, Climate Hazards Group InfraRed Precipitation with Stations; CR, Cross Ratio; ENSO, El Niño–Southern Oscillation; EODC, Earth Observation Data Centre, ESA, European Space Agency; FAO, Food and Agriculture Organization of the United Nations; FEWS NET, Famine Early Warning Systems Network GFM, Global Flood Monitoring; GMIA, Global Map of Irrigated Areas; H-SAF, EUMETSAT Satellite Application Facility on Support to Operational Hydrology and Water Management; IW, Interferometric Wide swath mode ITCZ, Intertropical Convergence Zone; MODIS, Moderate Resolution Imaging Spectroradiometer; NDVI, Normalized Difference Vegetation Index; SAR, Synthetic Aperture Radar; SSM, Surface Soil Moisture; WGS84, World Geodetic System 84

1. Introduction

Drought is a natural hazard characterized by prolonged water deficit (Palmer 1965). Drought typically begins as meteorological drought with below-average precipitation and high temperatures. It may then evolve into agricultural drought when soil moisture becomes insufficient for vegetation growth (Zhang et al. 2024). If soil moisture reaches the wilting point, plants lose their ability to extract water from the soil and experience physiological stress and potentially

CONTACT Carina Villegas-Lituma. Email: carina.villegas@tuwien.ac.at

plant death. Continued drought reduces streamflow and reservoir levels, leading to hydrological drought. Finally, socioeconomic drought occurs when water reserves cannot meet population demand (Zhang et al. 2022), which results in economic losses and social disruption.

These cascading drought stages have profound implications for rainfall-dependent farming regions. In Mozambique, severe droughts occur every four to five years and directly affect livelihoods, increasing poverty and food insecurity (World Bank 2024, 2011). Agriculture employs 79% of the workforce (International Center for Tropical Agriculture and World Bank 2017) and rainfall-dependent smallholders farm 96% of cultivated land (Silici, Bias, and Cavane 2015). This heavy reliance on rain-fed farming makes Mozambique particularly susceptible to drought, as recent events have shown: The 2015–2016 El Niño drought affected 1.5 million people and caused widespread crop failures across central and southern provinces (Ainembabazi, Rusike, and Keizire 2018; United Nations Office of the Resident Coordinator 2016). The 2019–2020 drought resulted in 75% below-average yields in southern regions (Famine Early Warning Systems Network 2020a). These recurring crises highlight the inadequacy of reactive response strategies.

Over recent decades, remote sensing has proven effective for vegetation monitoring in drought early warning systems (Senay et al. 2015). However, current operational systems rely primarily on optical vegetation indices, which have fundamental limitations. Optical sensors require solar illumination and clear atmospheric conditions. Clouds in particular impact observations or render imagery unusable (Zheng, Zhao, and Liu 2024; Sun et al. 2020; Jiang et al. 2021). This can distort statistical baselines used for anomaly detection, potentially generating false signals or masking actual drought events. The Normalized Difference Vegetation Index (NDVI) is the most widely used optical indicator. It quantifies vegetation greenness by detecting changes in photosynthetic activity as water availability declines (West, Quinn, and Horswell 2019; Camberlin et al. 2007). NDVI sensitivity to drought has been demonstrated across diverse environments including croplands and grasslands in the United States (Ji and Peters 2003), South African vegetation (Urban et al. 2018), and Mongolian forests and shrublands (Wei et al. 2022).

Despite this sensitivity, NDVI becomes unavailable in southern African agricultural regions during growing seasons due to peak cloud cover. During the 2015–2016 El Niño drought, Sentinel-2 acquired only 21 cloud-free observations over the South Africa–Mozambique border region between November 2015 and October 2017 (Urban et al. 2018). This gap is most severe from January to March, coinciding with the peak growing season (Global Information and Early Warning System on Food and Agriculture 2025). By April, when clouds dissipate, crop damage is often irreversible. Beyond observational limitations, NDVI presents fundamental constraints for rain-fed agricultural monitoring. As an indicator of greenness, NDVI responds primarily to visible canopy deterioration rather than progressive water stress propagating through the water cycle (Solgi, Ahmadi, and Seidel 2023). In countries like Mozambique, early warning systems based solely on NDVI may detect drought impacts only after crop losses have become irreversible.

Synthetic Aperture Radar (SAR) addresses these limitations using microwave wavelengths that penetrate clouds and atmospheric interference (Navalgund, Jayaraman, and Roy 2007). The Sentinel-1 constellation acquires dual-polarization (VV and VH), providing continuous observations throughout growing seasons. SAR backscatter responds to vegetation structure, biomass, and water content (Steele-Dunne et al. 2017). The VV polarization captures surface scattering and double-bounce reflections from soil and vertical structures, while VH polarization responds to volume scattering within vegetation canopies (Nairn and Brisco 2004). The cross-polarization ratio (CR = VH/VV) leverages this sensitivity by reducing soil moisture influences and emphasizing vegetation-specific changes (Vreugdenhil et al. 2020).

Studies demonstrate CR's responsiveness to crop phenology (Ma et al. 2024; Vreugdenhil et al. 2018), biomass dynamics (Arslan, Topakcı, and Demir 2022; Khabbazan et al. 2019), and water stress (Shorachi, Kumar, and Steele-Dunne 2022). These properties suggest CR may detect drought propagation from precipitation deficits through soil moisture depletion to vegetation stress, potentially providing complementary warning relative to optical indices. Shorachi, Kumar, and Steele-Dunne (2022) identified CR as an agricultural drought indicator in the Netherlands, finding that its dynamics reflected interactions among crop type, soil properties, and water management. However, CR applications for drought monitoring remain concentrated in

temperate regions with intensive agricultural systems. Its behaviour in tropical environments, characterized by diverse soils, mixed cropping, distinct phenology, and fragmented agricultural areas intermixed with dense natural vegetation, remains insufficiently characterized.

Critical questions regarding CR's effectiveness for tropical drought monitoring remain unanswered. The correspondence between CR and other drought-related variables (precipitation, soil moisture, optical indices) is poorly understood in tropical environments. Dense vegetation masking is theoretically necessary to isolate CR signals from rain-fed cropland fragmented within natural vegetation mosaics, yet its effectiveness has not been demonstrated—a critical gap given that rain-fed agriculture dominates smallholder farming across sub-Saharan Africa. Similarly, CR responses have not been compared between rain-fed and irrigated systems.

This study addresses these gaps by investigating drought-related responses of CR and NDVI over cropland in central and southern Mozambique during 2019–2024. We focus on six districts (Buzi, Chókwè, Govuro, Mabote, Massinga, and Muanza), spanning diverse soil types, rainfall regimes, and agricultural fields from homogeneous irrigated cropland to heterogeneous rain-fed areas. Specifically, we ask: (1) Does CR exhibit correspondence with NDVI across tropical land cover types? (2) Does dense vegetation masking improve CR-NDVI correspondence over agricultural areas, particularly in heterogeneous rain-fed areas with mixed land cover composition? (3) Does CR track drought propagation from precipitation deficit through soil moisture depletion to vegetation stress, capturing onset, progression, and recovery? Findings inform the integration of SAR-based indicators into agricultural early warning systems across southern and eastern Africa, where persistent cloud cover compromises the reliability of optical monitoring.

2. Materials and methods

2.1. Study area

Mozambique lies in southeastern Africa with tropical to subtropical climates and distinct wet and dry periods. The rainy and cyclone season occurs from November to April in the north and October to April in central and southern regions, coinciding with the warmest months. The dry season spans May to October in the north and April to September in the south, with June and July as the coolest months (Famine Early Warning Systems Network 2025; Food and Agriculture Organization of the United Nations 2021; Climate Centre 2024).

Mozambique's climate is shaped by mountainous topography (regionally), the Intertropical Convergence Zone (ITCZ), the Indian Ocean sea surface temperatures, and the El Niño–Southern Oscillation (ENSO), which strongly influences droughts, floods, and heatwaves (Tadross 2009; Climate Centre 2024). Soils vary regionally: sandy Arenosols dominate coastal areas, while inland soils include alluvial Fluvisols and Ferralsols in central regions and clay-rich Solonetz in the south (Dewitte et al. 2013).

This study analyse the spatial and temporal dynamics of Sentinel-1 CR across agricultural areas in six districts of central and southern Mozambique over the period 2019 to 2024: Buzi, Chókwè, Govuro, Mabote, Massinga, and Muanza (Figure 1). These districts have diverse agro-climatic conditions, with annual precipitation ranging from 674 mm in Chókwè to 1315 mm in Muanza, and mean land surface temperatures between 29.83 °C and 31.79 °C (Table 1). Farming systems vary across districts: Chókwè and Buzi are intensively irrigated; Mabote and Muanza are rain-fed; and Govuro and Massinga have no intensive irrigation. The analysed cropping area ranges from approximately 10 km^2 in Muanza to 311 km^2 in Chókwè.

Across all sites, the main growing season extends from October to February, with planting in October–November, vegetative growth through January, and reproductive stages culminating in a green harvest in February. A secondary growing season occurs in May and June, while the main harvest typically takes place between March and May (Food and Agriculture Organization of the United Nations 2021). The spatial distribution of the study sites, land cover, and irrigation infrastructure is shown in Figure 1, with detailed characteristics summarized in Table 1.

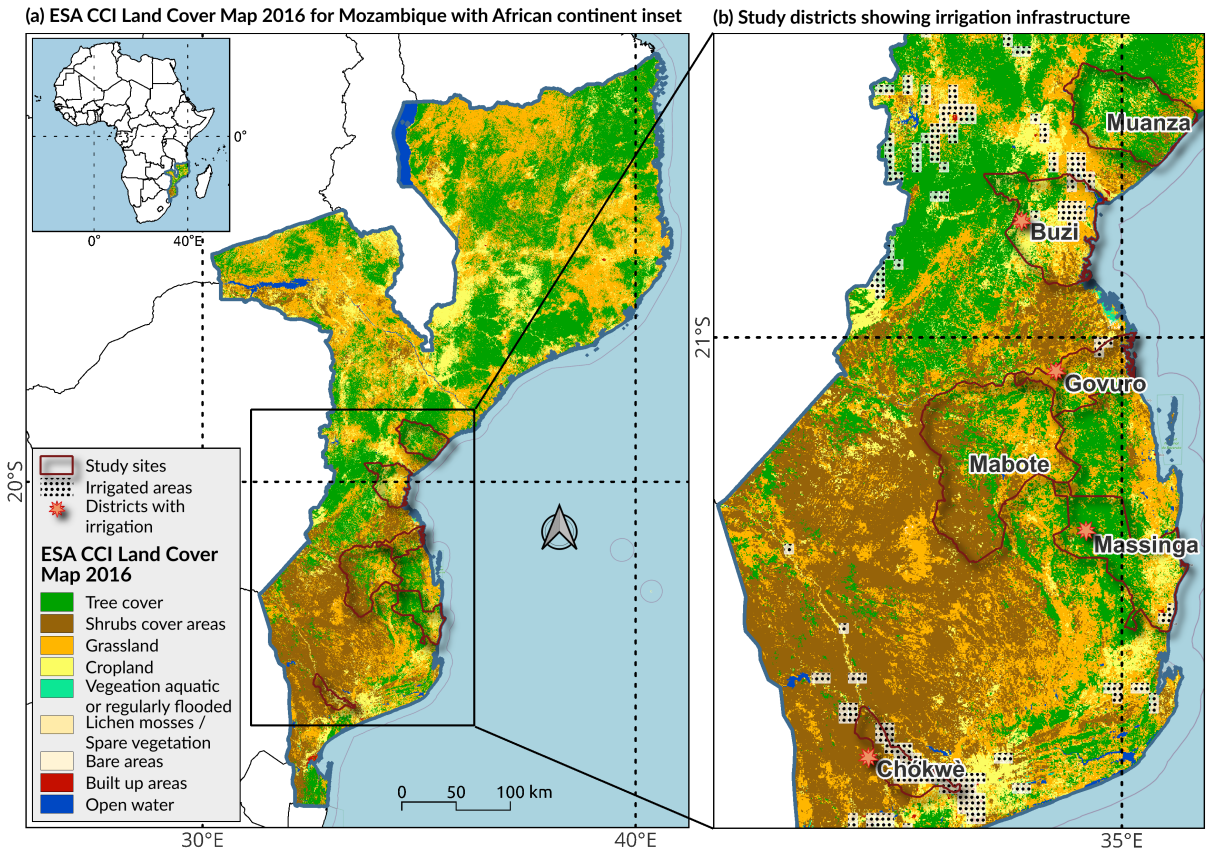

Figure 1. Map of the study area. (a) ESA CCI land cover map for 2016, depicting Mozambique with the African continent in the top. (b) District locations with irrigated areas based on the FAO Global Map of Irrigated Areas (GMIA v5).

Table 1. Adapted from Massart et al. (2025). Regional characteristics including mean precipitation derived from CHIRPS (1981–2023) and land surface temperature from MODIS (MOD11A1 Version 6).

District	Cropping Area (km^2)	Mean Annual Precipitation (mm)	Mean Land Surface Temperature (°C)	Farming System
Buzi	249.5	1134	31.78	Irrigated
Chókwè	311.0	674	31.79	Irrigated
Govuro	19.0	884	30.40	Rain-fed/Irrigated
Mabote	40.0	705	31.29	Rain-fed
Massinga	50.0	852	29.85	Rain-fed/Irrigated
Muanza	9.8	1315	29.83	Rain-fed

2.2. Datasets

All datasets used in this study were harmonized to a common spatiotemporal framework. Spatial data are reprojected to the World Geodetic System 84 (WGS84) (EPSG:4326) at a 500 m spatial sampling, and temporal data are aggregated into monthly composites for 2019-2024, unless otherwise specified.

2.2.1. Vegetation indicators

2.2.1.1 Sentinel-1 Cross Polarization Ratio

The Sentinel-1 constellation is part of the European Union's Copernicus program and consists of C-band SAR satellites operating at 5.405 GHz frequency. During the study period, Sentinel-1A and -1B provided observations every 6 days at the Equator. Following the decommissioning of Sentinel-1B in December 2021, only Sentinel-1A operated (12-day revisit), until Sentinel-1C

launched in December 2024, restoring the 6-day repeat cycle. All satellites provide backscatter data in VV and VH polarizations over land at Interferometric Wide swath mode (IW) with a 250 km swath. Backscatter observations are limited to descending orbits D152, D079, D035, D050, D006, and D108, and ascending orbit A057, as other orbits did not provide continuous coverage of the study area.

For this study, Sentinel-1 backscatter data at 20 m sampling, stacked in Equi7Grid, is acquired through the analysis-ready Sentinel-1 σ^0 datacube, as outlined by Wagner et al. (2021). A band-pass filter is applied to VV polarization (-19 dB $\leq \sigma^0 \leq -5$ dB) and VH polarization (-25 dB $\leq \sigma^0 \leq -11$ dB) to isolate vegetation backscatter and minimize contamination from water bodies and built-up surfaces. The filtered data are subsequently resampled to 500 m grid. The Sentinel-1 CR is then calculated by subtracting the VV from the VH polarization in the decibel domain (dB) (Equation 1); the resulting CR values are subsequently converted to linear scale to maintain consistency in the statistical treatment of all drought-related indicators.

$$CR = \sigma^0_{VH}[dB] - \sigma^0_{VV}[dB] \tag{1}$$

To capture CR signals from agricultural areas without contamination from surrounding dense vegetation, a masked CR product is also generated by applying the Dense Vegetation layer of the Global Flood Monitoring (GFM) dataset (Wagner et al. 2026) to the VV and VH polarizations prior to CR calculation. Pixels with $\geq 99\%$ coverage in this layer are excluded. The Dense Vegetation layer, at 20 m resolution, identifies woody vegetation using optimized thresholds from the Global Forest Change dataset and the Sentinel-1 Global Backscatter Model (for details, see EODC Public Wiki[1]).

2.2.1.2 Moderate Resolution Imaging Spectroradiometer (MODIS) NDVI

MODIS is carried onboard the National Aeronautics and Space Administration (NASA) Terra (EOS AM-1) and Aqua (EOS PM-1) satellites. Terra's orbit crosses the equator from north to south in the morning, while Aqua's orbit moves from south to north in the afternoon. This dual-satellite configuration allows observations of the same location one to two times per day. MODIS collects data across 36 spectral bands at varying spatial resolutions: 250 m for Bands 1-2, 500 m for Bands 3-7, and 1 km for Bands 8-36. Detailed data information and processing description are available on NASA's MODIS website[2].

The NDVI is expressed as $(\text{NIR} - \text{RED})/(\text{NIR} + \text{RED})$, where NIR and RED represent the reflectance values of the near-infrared and red bands, respectively. NDVI data are obtained from the Terra MODIS Vegetation Indices 16-Day product (MOD13A1) Version 6.1 with a native spatial resolution of 500 m. Data are accessed through the Application for Extracting and Exploring Analysis Ready Samples (AppEEARS) platform[3].

2.2.2. Water cycle variables

2.2.2.1 CHIRPS Precipitation

The Climate Hazards Group InfraRed Precipitation with Station data (CHIRPS) is a global rainfall dataset derived from a combination of infrared satellite data and ground station measurements. It provides precipitation estimates at a spatial resolution of 0.05° (∼5.5 km at the equator) across regions between 50 °S and 50 °N latitudes, available from 1981 in daily, 5-day (pentadal), 10-day (dekadal) and monthly temporal resolution (Funk et al. 2015). In this study, monthly precipitation data are obtained from CHIRPS Version 2.0[4].

[1] https://extwiki.eodc.eu/GFM/PDD/GFM_Product_Output_Layers

[2] https://modis.gsfc.nasa.gov/data/

[3] https://appeears.earthdatacloud.nasa.gov/

[4] https://data.chc.ucsb.edu/products/CHIRPS-2.0/

2.2.2.2 ASCAT Surface Soil Moisture (SSM) Climate Data Record

The Advanced SCATterometer (ASCAT) is a satellite-based scatterometer operated on the Metop-A, Metop-B, and Metop-C satellites. ASCAT employs two sets of three antennas covering 550 km-wide swaths and operates in the C-band at 5.255 GHz. Surface soil moisture is derived from ASCAT backscatter observations using the TU Wien change detection algorithm (Hahn, Melzer, and Wagner 2026). The resulting ASCAT Surface Soil Moisture Climate Data Record (CDR) product (H129), version 1 (v1), provides daily soil water content for the top 0–5 cm of the soil profile. Values are expressed as degree of saturation (0–100%) at a spatial sampling of 6.25 km on a Fibonacci grid (Hahn, Melzer, and Wagner 2026). The ASCAT SSM H129 v1 is distributed by the EUMETSAT Satellite Application Facility on Support to Operational Hydrology and Water Management (H SAF)[5]

2.2.3. Drought indicator

2.2.3.1 Standardized Z-Score of ASCAT Surface Soil Moisture

ASCAT soil moisture (H129) v1 observations are standardized using monthly z-scores to identify deviations from the long-term mean and to enable consistent comparisons of drought occurrence and intensity across regions and time. Monthly z-scores are calculated following Cammalleri et al. (2017) using Equation 2.

$$z_{x,i,k} = \frac{x_{i,k} - \mu_{x,i}}{\sigma_{x,i}} \tag{2}$$

where $x_{i,k}$ denotes the monthly mean soil moisture for month i in year k, with $\mu_{x,i}$ and $\sigma_{x,i}$ representing the corresponding long-term climatological mean and standard deviation. Standardized Z-score time series of ASCAT SSM are computed over an extended climatological reference period (2007–2024) to provide a robust baseline relative to the study period (2019–2024). Based on Z-score thresholds, agricultural drought conditions are classified as mild ($z > -1$), moderate ($-2 \leq z \leq -1$) and severe ($z < -2$)(Vreugdenhil et al. 2022).

2.2.4. Auxiliary data

2.2.4.1 ESA CCI Land cover map:

The European Space Agency (ESA) Climate Change Initiative (CCI)[6] 2016 map provides land cover classification at a 20 m resolution in WGS84. The map categorizes land into 10 classes based on Sentinel-2A imagery: tree cover, shrubs, grassland, cropland, aquatic or regularly flooded vegetation, lichen and mosses or sparse vegetation, bare areas, built-up areas, snow and/or ice, and open water. For this study, the ESA CCI Land Cover 2016 map is resampled to a 500 × 500 m pixel resolution using the mode aggregation method.

2.2.4.2 FAO Global Map of Irrigated Areas

The Food and Agriculture Organization of the United Nations (FAO) Global Map of Irrigated Areas (GMIA)[7] v5.0 provides irrigation extent at 5 arc-minutes resolution (∼9 km) and represents conditions based on AQUASTAT statistics for the year 2005. Cropland pixels with more than 20% irrigated area fraction were classified as irrigated; others as rain-fed. The dataset reflects irrigation patterns have shown minimal change since 2005.

[5] https://hsaf.meteoam.it/Products/Detail?prod=H129

[6] https://2016africalandcover20m.esrin.esa.int/

[7] https://www.fao.org/aquastat/en/geospatial-information/global-maps-irrigated-areas/latest-version

2.3. Methods

2.3.1. CR and NDVI correspondence and vegetation masking

To assess CR-NDVI correspondence across land cover types and evaluate the effectiveness of dense vegetation masking, a two-part analysis is conducted.

First, mean values of NDVI, masked CR, and unmasked CR are mapped across Mozambique to visualize their spatial distributions and examine the effect of masking across land cover types.

Second, temporal Pearson correlation coefficients are calculated between CR and NDVI for each pixel. Analysis is performed using two CR datasets: unmasked CR, evaluated without vegetation filtering, and masked CR, where dense vegetation pixels are excluded using the GFM Dense Vegetation Mask. Correlations are stratified by land cover class (cropland, grassland, shrubland, tree cover) using the ESA WorldCover 2021 map. If masked CR demonstrates stronger correlation with NDVI over agricultural areas, it is adopted for all subsequent analyses.

2.3.2. Drought cascade from rainfall to vegetation

Following results from Section 2.4.1, CR (dense vegetation masked) is used for all subsequent analyses. To assess drought propagation from precipitation through soil moisture to vegetation, a three-part analysis is conducted.

First, pixel-wise Pearson correlations are calculated between vegetation indicators (CR, NDVI) and precipitation and soil moisture. Correlations are stratified by land cover type to assess vegetation-water relationships along the drought cascade. Second, yearly anomalies are computed to track drought propagation through the precipitation-vegetation pathway. For each calendar year (2019–2024), anomalies are calculated as deviations from the 2019–2024 mean for precipitation (CHIRPS), soil moisture (ASCAT), NDVI, and masked CR. Spatial patterns are compared across indicators to assess correspondence during drought and recovery periods. To quantify drought impacts over agricultural areas, CR anomalies are extracted for cropland pixels (ESA CCI land cover class 4) within the six study districts and summarized as district-level annual means. Third, vegetation response to drought is assessed at regional scale. Time series of precipitation, soil moisture, NDVI, and CR are extracted for the study sites. Precipitation and soil moisture are averaged at district level, while NDVI and masked CR are extracted over cropland only. Drought periods are identified using soil moisture z-scores. NDVI and CR dynamics are compared between drought and non-drought years to evaluate sensitivity and recovery patterns.

3. Results

3.1. CR-NDVI correspondence and dense vegetation masking

Figure 2 shows pixel-wise temporal averages (2019-2024) of NDVI (a) and CR without (b) and with (c) the Dense Vegetation Mask across Mozambique. NDVI ranges from $\sim$0.45 to $\sim$0.70, with the highest values in central and northern regions dominated by tree cover. Croplands have intermediate values, while grassland and shrubland exhibit lower NDVI values. Both masked and unmasked CR range from $\sim$0.21 to $\sim$0.27. For unmasked CR, tree-covered areas display moderate CR values, whereas shrublands show higher CR values. Grassland and cropland exhibit low and moderate CR values, respectively. After applying the Dense Vegetation Mask, dense forest is excluded. CR values over shrublands remain similar to unmasked values, while cropland and grassland show lower values.

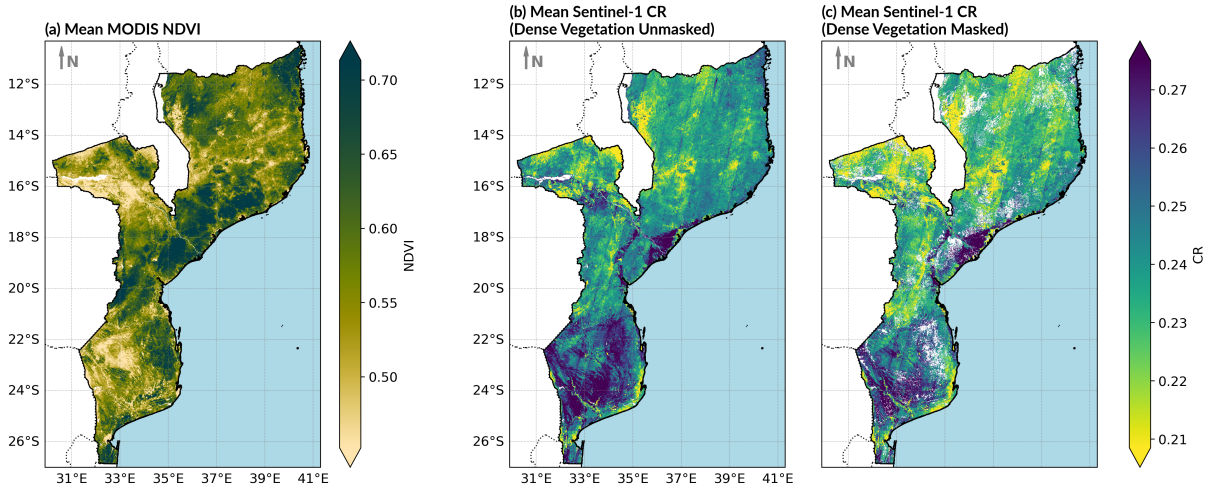

Figure 2. Mean NDVI (a) and CR without (b) and with (c) Dense Vegetation Mask across Mozambique for 2019–2024. Black outlines show study sites.

To investigate the relationship between NDVI and CR over time, Pearson correlation is computed for each pixel across Mozambique. The resulting temporal correlation maps for both unmasked and masked CR (Figure 3a,c) show distinct patterns, with positive and negative correlations varying by land-cover type (Figure 3b,d). With unmasked CR, cropland exhibits the most consistently positive correlations, with a median of 0.49 and an interquartile range of 0.10–0.67. Most cropland pixels (79%) show positive correlations, and 36.5% exhibit strong correlations (>0.6). Grassland also shows positive correlations, though weaker (median=0.26) and more variable (66% positive, 33% negative). In contrast, tree and shrub cover display weak or negative correlations with high variability. Tree cover has the lowest median correlation (−0.11), with 42% of pixels showing negative correlations. Correlation across shrub cover is nearly evenly split (55% negative, 45% positive), with a median close to zero (−0.09). To isolate agricultural areas, the GFM Dense Vegetation Mask is applied. After masking, correlations improve across all land cover types. Cropland shows the strongest improvement, with a median correlation of 0.60 and 91.6% of pixels displaying positive correlations. Grassland reaches a median of 0.51. Tree cover shifts to predominantly positive values (median=0.44), with approximately 300,000 dense forest pixels removed. Shrub cover improves but remains low (median=0.15), with 60.2% of pixels showing positive correlation.

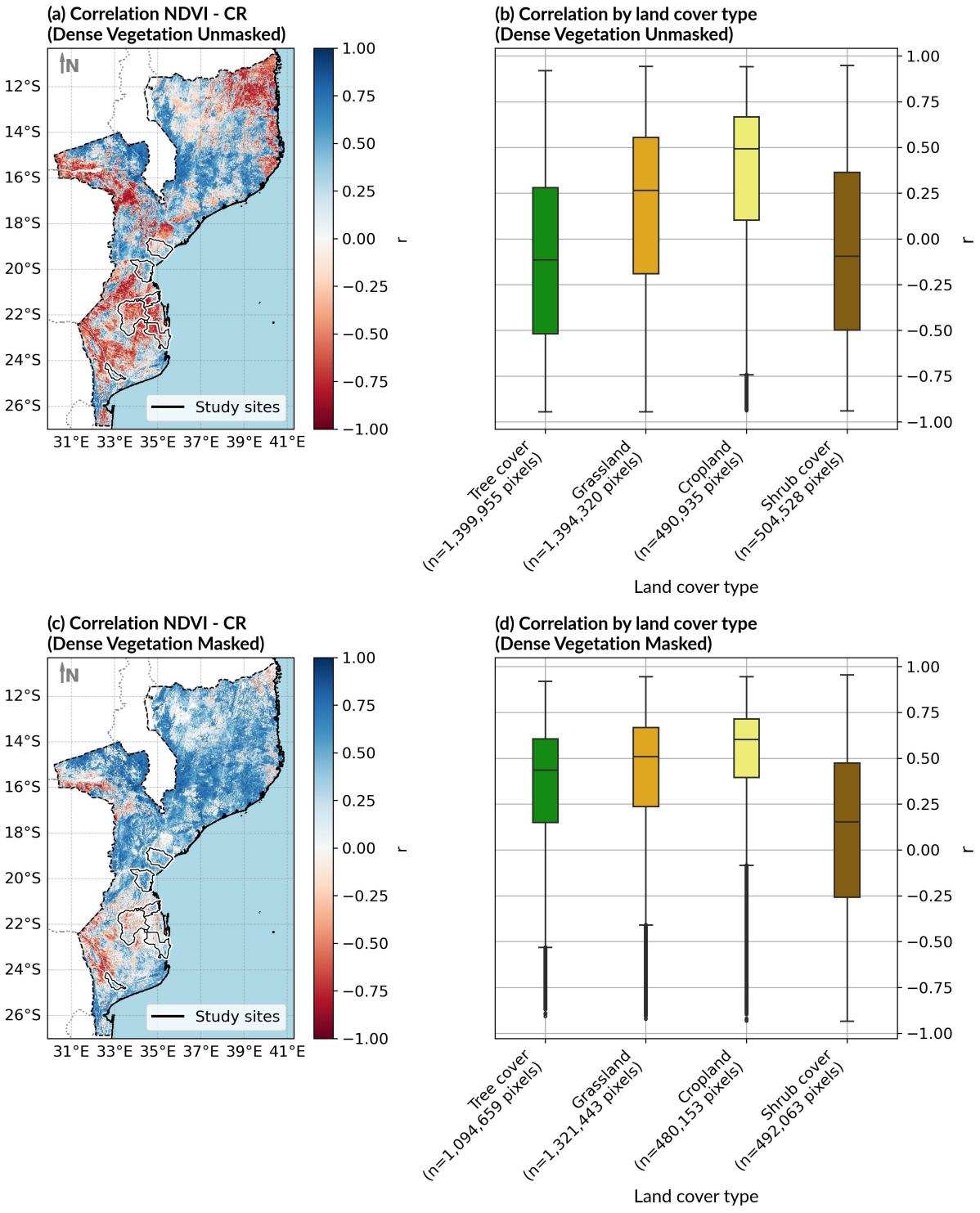

Figure 3. Pearson correlation between NDVI and CR for (a) unmasked and (c) masked dense vegetation, with (b,d) corresponding distributions by ESA CCI land cover class. Boxplots show median (line), interquartile range (box), 1.5× Interquantile Range (whiskers), and outliers (points). Sample sizes (n) are pixel counts. Dashed line shows national boundary; solid outlines show study sites.

3.2. Drought cascade from rainfall to vegetation response

3.2.1. Relationships along the drought cascade

The relationship between vegetation and hydrological variables along the drought cascade is quantified using Pearson correlations for 2019–2024 (Figure 4). Correlation strength varies by

land cover (Table 2). NDVI shows consistently strong correlations with soil moisture across all land cover types (r=0.47–0.73), with strong correlation over cropland (r=0.63). CR correlations are more variable: moderate over cropland (r=0.36) but stronger over grassland and forest (r=0.66 and 0.67, respectively). In shrublands, CR correlates more strongly with precipitation (r=0.66) than with soil moisture (r=0.58).

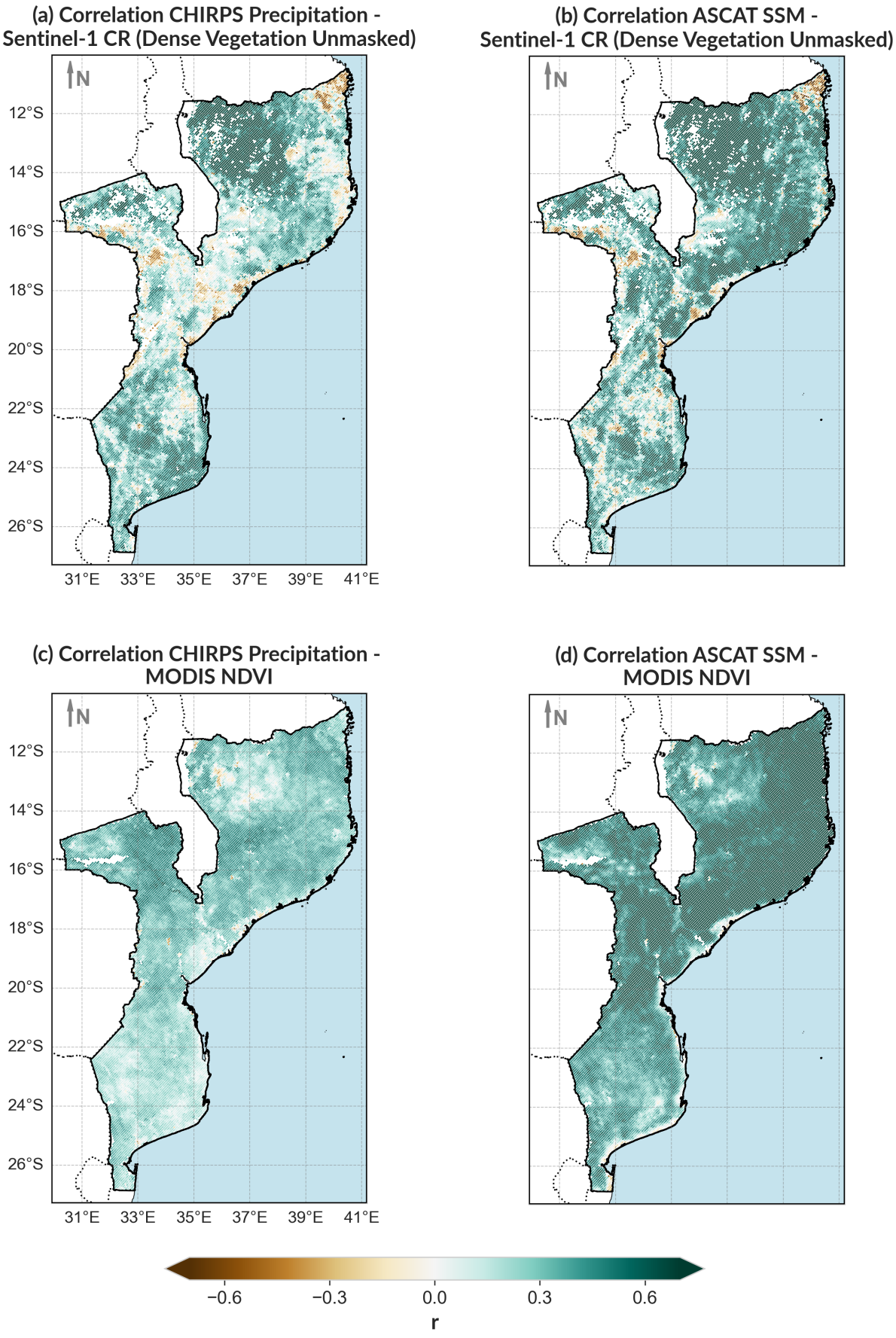

Figure 4. Pearson correlation of (a,b) Sentinel-1 CR (dense vegetation masked) and (c,d) MODIS NDVI with CHIRPS precipitation and ASCAT soil moisture, respectively.

Table 2. Pearson correlation coefficients between variables across land cover types (2019–2024), computed at 6.25 km resolution. CR = Sentinel-1 Cross Ratio (Dense Vegetation Masked); NDVI = MODIS Normalized Difference Vegetation Index; SSM = ASCAT Surface Soil Moisture; Precipitation = CHIRPS Precipitation. All correlations are significant at $p < 0.001$, except: Shrubland (NDVI – Precipitation: $p < 0.01$); Cropland (CR – SSM: $p < 0.01$; CR – Precipitation: $p = 0.065$).

	Correlation			
Land Cover	CR – SSM	CR – Precipitation	NDVI – SSM	NDVI – Precipitation
Forest	0.67	0.45	0.73	0.44
Shrubland	0.58	0.66	0.47	0.33[a]
Grassland	0.66	0.46	0.70	0.47
Cropland	0.36[b]	0.22[c]	0.63	0.46

[a] $p < 0.01$; [b] $p < 0.01$; [c] $p = 0.065$. All other correlations significant at $p < 0.001$.

3.2.2. Drought propagation

Yearly anomalies of precipitation, soil moisture, NDVI, and CR (dense Vegetation masked) are calculated from 2019 to 2024 to examine drought propagation patterns spatially (Figure 5). Spatial patterns of precipitation and soil moisture anomalies show general consistency, though the spatial coverage of each anomaly varied across regions. In 2019, both variables exhibit negative anomalies across the south and positive anomalies extending from the central to northern regions. In 2020, negative anomalies of both precipitation and soil moisture correspond spatially across most of the region, except for eastern Mozambique. In 2021, precipitation and soil moisture show positive anomalies dominating the south and central regions, while the north remains negative. In 2022, precipitation displays positive anomalies in the north and negative anomalies in the south and parts of the central region. Soil moisture anomalies exhibit considerable spatial heterogeneity, with mixed patterns of positive and negative anomalies across the country. In 2023, moderate negative precipitation anomalies affect central and northern regions and are partially mirrored by soil moisture. The south predominantly shows positive anomalies for both precipitation and soil moisture, though a localized patch of strong negative soil moisture anomaly is evident in the southern region. In 2024, negative precipitation anomalies intensify across the country. Soil moisture largely corresponds with these, except for patches of positive anomalies in the northern areas.

NDVI anomalies broadly reflect these soil moisture patterns across the study period. In 2019, correspondence is strongest in the south where anomalies are most pronounced, before extending across the entire country in 2020. In 2021, NDVI shows recovery in the south, while negative anomalies persist in the north. From 2022 to 2023, NDVI broadly tracks soil moisture patterns, though NDVI anomalies are more spatially extensive in the central and northern regions. In 2024, NDVI-soil moisture correspondence is evident only in the eastern areas, where both exhibit negative anomalies.

CR anomalies correspond spatially with both soil moisture and NDVI, with stronger agreement observed with NDVI. From 2019 to 2020, CR anomalies transition from mixed patterns in the south to predominantly negative anomalies country-wide, mirroring soil moisture and NDVI patterns. In 2021, CR shows negative anomalies in northern regions, while central and southern areas exhibit mixed patterns with both positive and negative anomalies. From 2022 to 2023, correspondence with soil moisture is evident in northern regions, while the south exhibits weaker and mixed anomalies with localized negative patches. In 2024, intense negative CR anomalies are more spatially extensive in central and northern regions compared to NDVI patterns, with recovery continuing in the south.

To examine drought propagation over cropland more specifically, CR anomalies are extracted within the six study districts (Figure 6). All districts experience negative CR anomalies during 2019–2020, with 2020 the most severe year (6b) and Mabote and Massinga being the most affected.

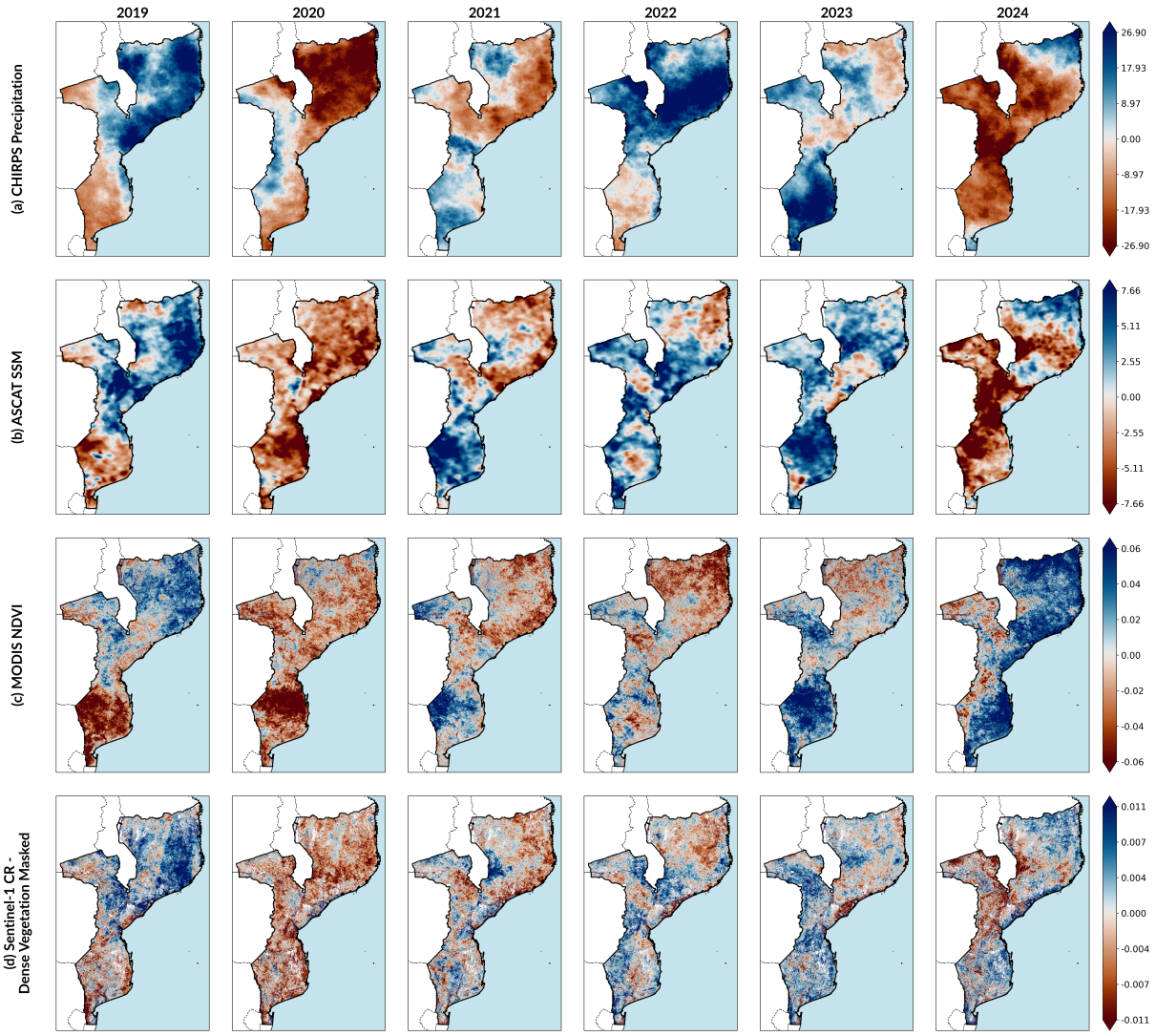

Figure 5. Yearly anomalies of (a) CHIRPS precipitation, (b) ASCAT surface soil moisture, (c) MODIS NDVI, and (d) Sentinel-1 CR (dense vegetation masked) for 2019–2024. Anomalies represent deviations from the period mean.

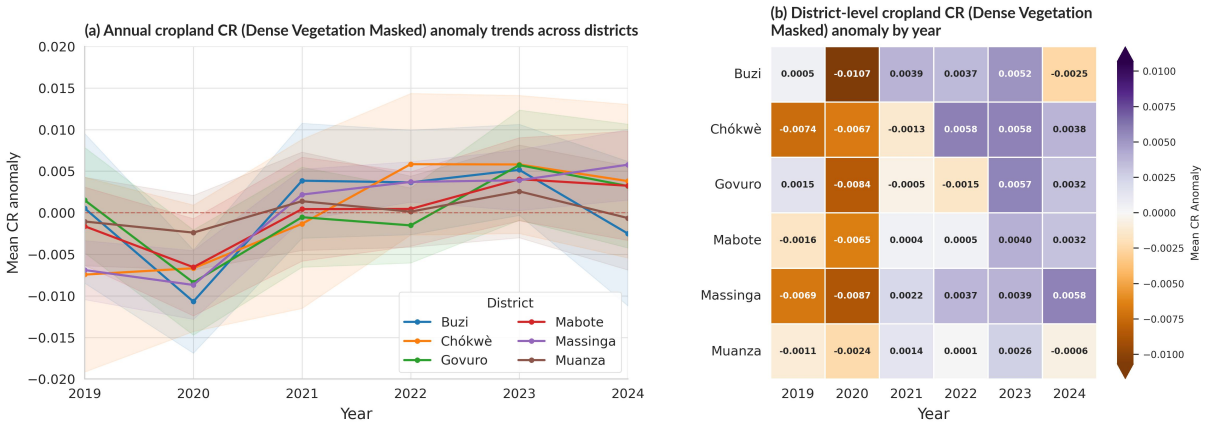

Figure 6. Annual Sentinel-1 CR anomalies over cropland in six Mozambique districts (2019–2024). (a) District mean time series (solid lines) with shaded bands showing ±1 standard deviation across pixels; red dashed line marks zero. (b) Annual heatmap illustrates positive and negative anomalies. CR values exclude dense vegetation.

3.2.3. Temporal dynamics

For the six districts, temporal dynamics of precipitation, soil moisture, NDVI, and CR (dense vegetation masked) are presented in Figures 7 and 8. The central districts (Buzi, Muanza) receive the highest precipitation per rainy season (897 mm and 990.5 mm, respectively). Massinga and Govuro receive moderate precipitation (682 mm each), while Mabote (558 mm) and Chókwè (551 mm) receive the lowest amounts. Soil moisture broadly tracks precipitation, but the relationship varies by district. Buzi shows the highest soil moisture. Muanza, despite the highest precipitation, shows lower soil moisture. Govuro displays moderate soil moisture, with a notable response to precipitation variability. Chókwè maintains relative high soil moisture even with low precipitation. Mabote and Massinga display the lowest soil moisture.

NDVI increases shortly after soil moisture rises at the start of the growing season across all districts. CR seasonal dynamics, however, vary with water input. In districts with higher water input (Buzi, Chókwè), both NDVI and CR display strong seasonal amplitude, though CR peaks after NDVI. Buzi and Muanza show the largest CR seasonal amplitudes, followed by Chókwè, while water-limited districts (Govuro, Mabote, Massinga) exhibit lower CR amplitudes despite pronounced NDVI seasonality.

ASCAT SSM z-scores are used to identify drought periods across the study area (Figures 7 and 8). A severe drought occurs during 2019/2020. Mabote, Massinga, Muanza and Govuro experienced the strongest and most persistent negative z-scores, while Buzi and Chókwè exhibit moderate drought conditions. Soil moisture recovers across most districts from 2020/2021 through early 2024. A secondary drought in 2021/2022 affects Buzi and Govuro, while Chókwè and Muanza maintain alternating patterns with shorter drought-recovery cycles. By late 2024, negative z-scores in Mabote, Buzi, and Chókwè indicate a new drought period.

A clear vegetation drought response is evident: both NDVI and CR show reduced peaks during 2019/2020 compared to subsequent wet years. Impact severity varies by district. In Buzi, both NDVI and CR show reduced amplitude but maintain visible growing season patterns. Chókwè presents reduction in amplitude of NDVI but not CR. Muanza shows reduced CR amplitude but not NDVI. Govuro, Mabote, and Massinga are most severely affected, showing reduced NDVI peaks. In these districts, CR shows limited seasonality throughout the study period, with drought appearing as signal flattening rather than as a deviation from seasonal patterns.

Following the 2019/2020 drought, NDVI and CR recovery varies across districts depending on water supply. In Buzi, CR exceeds pre-drought levels during subsequent wet periods, while Chókwè shows more gradual recovery. In Muanza, CR recovers until a secondary drought in 2023. In water-limited districts (Govuro, Mabote, Massinga), CR shows weak seasonal patterns throughout the study period, despite clear NDVI seasonality.

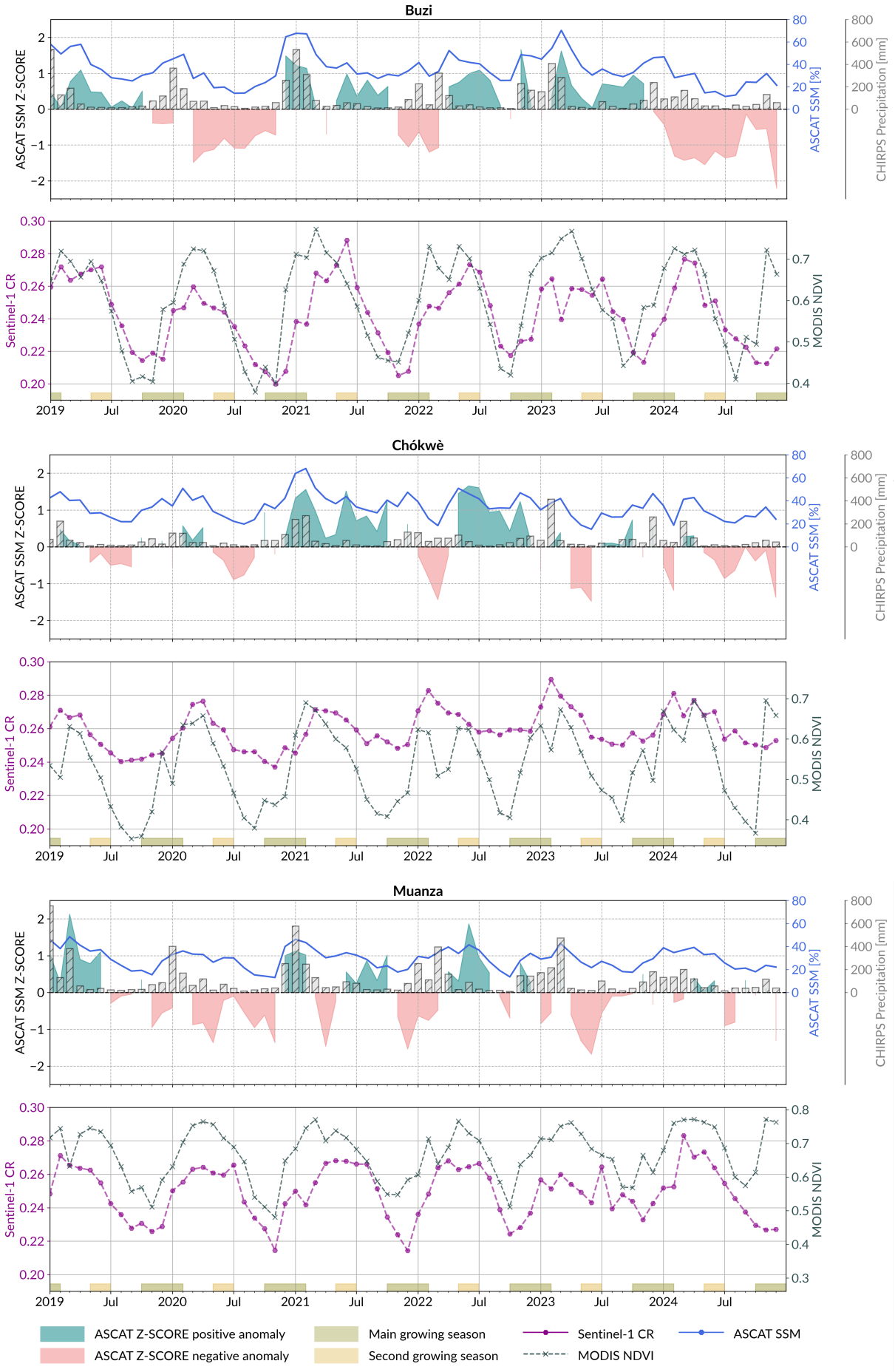

Figure 7. Time series showing CHIRPS precipitation (grey bars), ASCAT soil moisture Z-score (top panel), with positive anomalies shaded in teal and negative anomalies in coral, alongside ASCAT surface soil moisture (blue lines) at district level. The bottom panel shows the monthly means of Sentinel-1 CR (fuchsia lines) and MODIS NDVI across cropland (green lines).

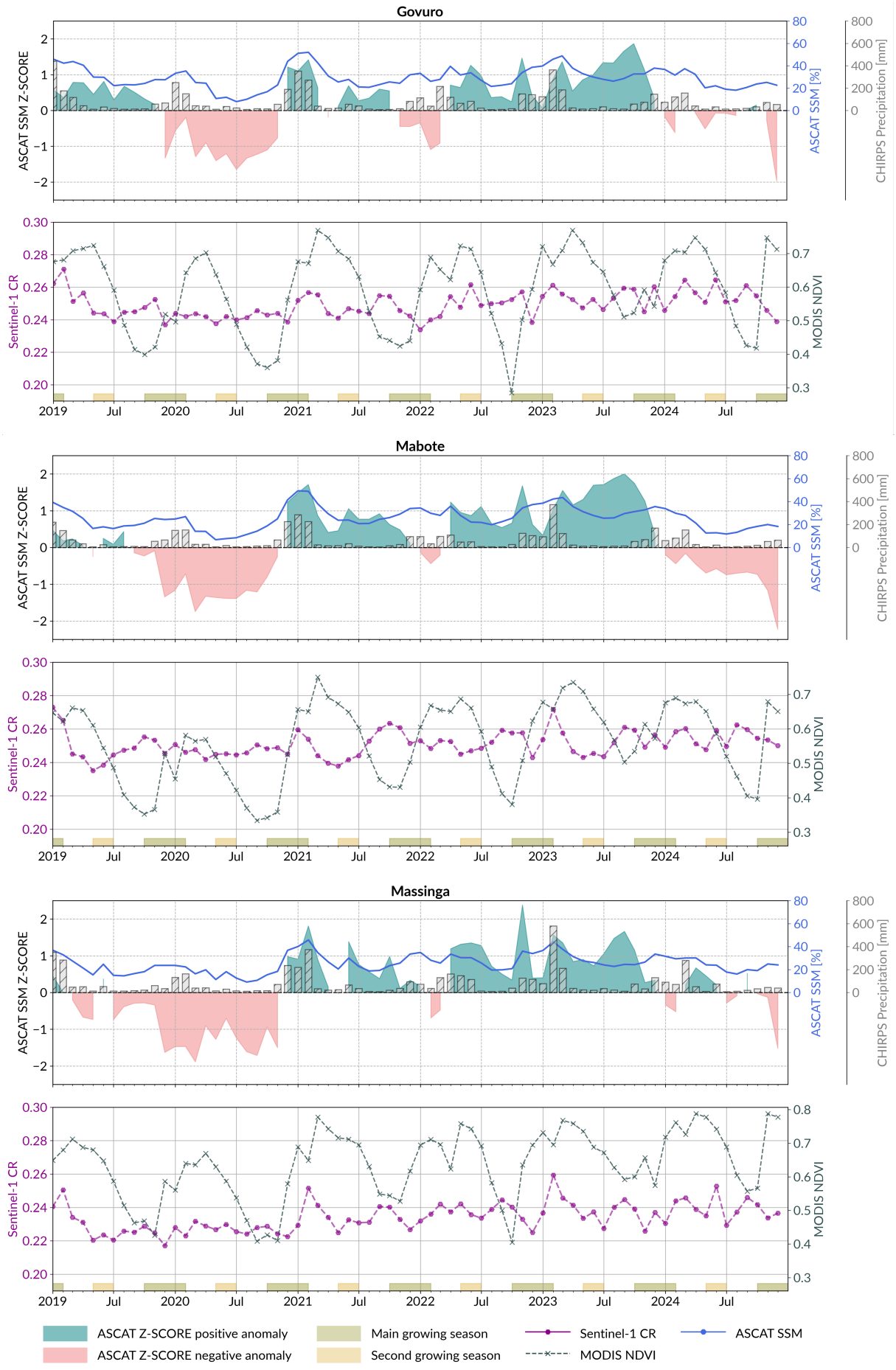

Figure 8. Time series showing CHIRPS precipitation (grey bars), ASCAT soil moisture Z-score (top panel), with positive anomalies shaded in teal and negative anomalies in coral, alongside ASCAT surface soil moisture (blue lines) at district level. The bottom panel shows the monthly means of Sentinel-1 CR (fuchsia lines) and MODIS NDVI across cropland (green lines).

4. Discussion

4.1. Vegetation masking strengthens CR-NDVI correspondence over tropical cropland

This study confirms that CR exhibits temporal correspondence with NDVI over tropical agricultural land, extending findings from European cropland and grassland (Veloso et al. 2017; Holtgrave et al. 2020), where CR-NDVI correspondence highlighted the complementarity of optical and SAR observations, but also reveal the need of dense vegetation masking when we want to focus in drought monitoring across agricultural systems and mitigate effects of food insecurity, but also highlight the need for dense vegetation masking to support drought monitoring over agricultural systems. Without masking, cropland shows the strongest correspondence (median r=0.49), while forest and shrubland present the lowest median correlations (-0.11 and -0.09, respectively), reflecting structural changes during phenological transitions that weaken CR-NDVI correspondence (Yu et al. 2023). After masking, CR-NDVI correspondence over cropland substantially improves: the proportion of pixels with positive correlations increased from 79% to 91.6%, and median correlation from 0.49 to 0.60. This reflects the removal of dense forest signals, which respond differently to seasonal dynamics than agricultural vegetation.

Beyond cropland, the persistence of positive correlations over tree cover and shrubland before and after masking indicates that sparser canopies and mixed herbaceous vegetation also contribute to positive CR-NDVI correspondence (Frison et al. 2018; Vreugdenhil et al. 2020). The modest change in shrubland median correlation (-0.09 to 0.15) suggests that the most shrubland pixels are not classify as dense vegetation and are therefore retained after masking, consistent with the spatial agreement between the ESA CCI Land Cover map and the GFM Dense Vegetation Mask at 20 m resolution. Overall, these results demonstrate that vegetation masking reduces forest signal contamination and strengthens CR-NDVI correspondence over agricultural land, supporting the use of CR for crop monitoring in tropical landscapes.

4.2. CR tracks drought propagation from precipitation through soil moisture to vegetation

While the linear response of NDVI to rainfall is well established (Maselli 2004; Hussain et al. 2023; Wang, Rich, and Price 2003; Richard and Poccard 1998; Toté et al. 2015), our analysis shows that NDVI anomalies correspond more closely with soil moisture than with precipitation, consistent with the stronger NDVI-root zone soil moisture correlation (Sazib, Mladenova, and Bolten 2020; Ibrahim et al. 2015). CR similarly corresponds more strongly with soil moisture than precipitation across most land cover types, though its sensitivity is more variable (Table 2). Over cropland, CR correspondence is weaker, likely because CR is more sensitive to canopy structural changes associated with phenological development than to vegetation water content alone (Vreugdenhil et al. 2018). In shrubland, the stronger CR correlation with precipitation is consistent with canopy rainfall interception limiting the water that reaches the soil (Domingo et al. 1998; Zwieback et al. 2019; Chang 2020). A similar interception effect is evident in Muanza: despite receiving the highest precipitation among the study sites, this district shows comparatively low soil moisture (Figures 7), likely due to its extensive tree cover (Figure 1), which increases evapotranspiration and canopy interception. Soil moisture-vegetation correspondence is evident in the national-scale anomaly patterns (Figure 5). During the 2019/2020 El Niño drought (Alemaw 2022), negative anomalies propagated from precipitation through soil moisture to vegetation across most of the country. This correspondence weakened in 2024 due to overlapping factors: prolonged El Niño conditions (Moses et al. 2025; Famine Early Warning Systems Network 2024) and multiple tropical storms and cyclones, including Alvaro (January), Filipo (March), and Chido (December) (United Nations Office for the Coordination of Humanitarian Affairs 2024b,a; European Commission's Directorate-General for European Civil Protection and Humanitarian Aid Operations 2024). These events brought localized rainfall across Nampula, Zambézia, Sofala, Inhambane, Gaza, Maputo, spanning two growing seasons (2023/2024 and

2024/2025), adding temporal complexity to the 2024 calendar-year anomaly distributions.

At the regional scale, CR anomalies confirm the capacity to detect drought propagation over the six study districts, with the most severe effects recorded in 2019 and 2020 (Figure 6), in line with FEWS NET reports of extended dry spells and below-average rainfall across central and southern Mozambique (Famine Early Warning Systems Network 2020a,b). These findings are broadly consistent with European observations of backscatter reductions during drought (Meroni et al. 2021), although direct comparisons should be interpreted cautiously given the differences in field size, crop heterogeneity, and management intensity between Mozambican and European agriculture. Overall, these results confirm CR's capacity to track agricultural drought through the water cycle, consistent with its responsiveness to biomass and vegetation water content (Vreugdenhil et al. 2018).

4.3. Water availability and land cover composition shape CR drought sensitivity: implications for early warning

Correlation analysis over cropland (Table 2) revealed that both NDVI and CR correspond more closely with soil moisture than with precipitation. Temporal analysis confirms this dependency while revealing differences in timing of the two indicators. NDVI increases shortly after soil moisture rises at the start of the growing season across all districts. CR seasonal dynamics, however, vary with water availability. In districts with higher water input (Buzi, Chókwè), both NDVI and CR display strong seasonal amplitude. CR peaks after NDVI in these districts, reflecting the different vegetation properties captured by each indicator: NDVI responds to chlorophyll content at green up, while CR responds to vegetation water content and canopy development (Vreugdenhil et al. 2020).

CR drought response varied between water-abundant and water-limited districts. In Buzi, the slight CR reduction during 2019/2020 reflects decreased crop water content and biomass (Shorachi, Kumar, and Steele-Dunne 2022). In Chókwè, irrigation maintained seasonal amplitude throughout the drought, effectively masking its effects on CR. In districts where cropland is interspersed with substantial natural vegetation cover (Govuro, Mabote, Massinga, Muanza), the attenuated CR signal raises the question of whether it reflects genuine drought impact or signal contamination from non-cropland land cover. Land cover fraction analysis at 20m̃ resolution (Figure 9, Govuro shown as representative example) reveals that cropland-dominant pixels represent a minority in Govuro, Mabote, Massinga, and Muanza, while shrubland and forest dominate, causing district-averaged CR time series to integrate mixed phenological signals that partially obscure cropland-specific drought responses. Stratified analysis confirms that cropland-only pixels show distinct seasonal dynamics, indicating that the muted signal reflects land cover heterogeneity rather than CR insensitivity to drought. In Buzi and Chókwè, NDVI also showed reduced seasonal amplitude during drought years. These findings align with studies documenting NDVI reductions of 3–4% in cropland during drought periods (Gidey et al. 2018), confirming NDVI's effectiveness for monitoring prolonged stress (Liu et al. 2018; Solgi, Ahmadi, and Seidel 2023). However, without land cover stratification at higher resolution, NDVI cannot distinguish whether the observed stress originates from cropland or surrounding natural vegetation. Post-drought recovery depends on the water input each district receives, whether from precipitation or irrigation, as illustrated by the relatively rapid recovery in Buzi and Chókwè.

Beyond signal characterization, these findings have implications for integrating CR into drought early warning. The main challenge is not CR's drought sensitivity but isolating the cropland signal within heterogeneous landscapes. This challenge applies equally to CR and NDVI, as both integrate mixed land cover signals at moderate resolution. High-resolution land cover stratification can filter cropland-dominant pixels for either indicator, but the benefit differs: CR's sensitivity to vegetation structure means that cropland, shrubland, and forest produce distinct backscatter dynamics, so stratification effectively separates these signals. NDVI's greenness response is less structurally specific, so crop and tree canopies produce similar signals even after filtering. Furthermore, CR provides continuous monitoring in cloud-prone tropical regions

where NDVI observations are frequently unavailable. In tropical smallholder landscapes, where rain-fed agriculture and woody vegetation coexist at fine spatial scales, combining land cover stratification with CR's structural sensitivity offers a pathway toward more targeted drought information for food-insecurity.

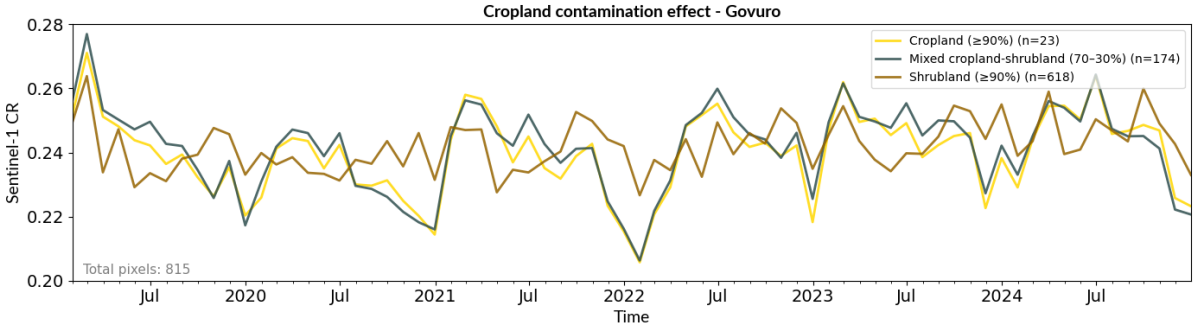

Figure 9. Sentinel-1 CR time series for Govuro district showing the effect of land cover composition at 20 m resolution. Lines represent mean CR across pixels with different cropland fractions: pure cropland ($\geq$90%, n=23), mixed cropland–shrubland (70–30%, n=174), and shrubland-dominated ($\geq$90%, n=618).

5. Conclusions

This study systematically examined Sentinel-1 CR as an agricultural drought indicator in tropical Mozambique from 2019 to 2024. The main conclusions are:

- CR and NDVI are complementary for agricultural drought monitoring. After applying dense vegetation masking, CR-NDVI correlations were strongly positive over cropland (median r = 0.60, with 91.6% of pixels showing positive correlations), confirming the value of combining radar and optical observations.
- Vegetation drought response corresponded more closely with soil moisture than with precipitation across most land cover types, though shrubland showed stronger precipitation dependence, likely reflecting canopy interception effects.
- CR interpretation depends on land cover composition. Cropland-dominated areas yield clear seasonal signals suitable for drought detection, but in heterogeneous cropland-forest/shrub mosaics, typical of rain-fed agricultural systems, dense vegetation masking alone is insufficient: the GFM mask removes forest but retains shrubland and open woodland, which introduce non-cropland signals. Land-cover-stratified analysis at high resolution is therefore required to complement masking and isolate cropland-specific responses.
- CR tracked drought propagation from precipitation through soil moisture to vegetation during the 2019/2020 El Niño, and captured subsequent recovery, confirming its capacity to monitor drought evolution through the water cycle.

These findings support the integration of CR into multi-indicator drought early warning systems for sub-Saharan Africa. CR complements precipitation, soil moisture, and optical indices through its responsiveness to canopy structure and its capacity for continuous monitoring regardless of cloud cover. Future applications should incorporate higher-resolution land cover stratification and masking approaches tailored to tropical agricultural mosaics.

Acknowledgments

This publication was supported by TU Wien Bibliothek through its Open Access funding programme.

Funding sources

This research was supported by the Austrian Development Agency under the DrySat project [grant number: 2789-00/2022].

Declaration of interest statement

The authors report no conflict of interest.

Declaration of Generative AI and AI-assisted technologies

Claude (Anthropic, claude.ai) was used to assist with language editing during the writing of this manuscript. All content was subsequently reviewed and revised by the authors, who take full responsibility for the published work.

CRediT authorship contribution statement

Carina Villegas-Lituma: Conceptualization, Data curation, Formal analysis, Investigation, Methodology, Visualization, Writing – original draft, Writing – review & editing. **Mariette Vreugdenhil:** Conceptualization, Writing – original draft, Writing – review & editing, Supervision. **Samuel Massart:** Writing – review & editing. **Ignacio Borlaf-Menal:** Data curation, Writing – review & editing. **Bernhard Raml:** Data curation (Sentinel-1 CR processing), Writing – review & editing. **Rafael Rogério Borguete:** Writing – review & editing. **Wolfgang Wagner:** Writing – review & editing, Supervision.

Data availability statement

The datasets used in this study are described in the Data and Methods section. Sentinel-1 CR data were processed by the authors and are available upon reasonable request from the corresponding author.

References

Ainembabazi, John Herbert, Joseph Rusike, and Boaz Keizire. 2018. *The 2015-16 El Niño-induced drought crisis in Southern Africa: Lessons from Historical Data and Policy Implications*. Technical Report. Alliance for a Green Revolution in Africa. `https://agra.org/wp-content/uploads/2020/08/AGRA-drought-crisis-in-Southern-Africa_v2-.pdf`.

Alemaw, Berhanu F. 2022. "The Recent Droughts of 2019/20 in Southern Africa and Its Teleconnection with ENSO Events." *Atmospheric and Climate Sciences* 12: 246–263. https://doi.org/10.4236/acs.2022.122015.

Arslan, Ibrahim, Mehmet Topakcı, and Nusret Demir. 2022. "Monitoring Maize Growth and Calculating Plant Heights with Synthetic Aperture Radar (SAR) and Optical Satellite Images." *Agriculture (Switzerland)* 12. https://doi.org/10.3390/agriculture12060800.

Camberlin, P., N. Martiny, N. Philippon, and Y. Richard. 2007. "Determinants of the interannual relationships between remote sensed photosynthetic activity and rainfall in tropical Africa." *Remote Sensing of Environment* 106: 199–216. https://doi.org/10.1016/j.rse.2006.08.009.

Cammalleri, Carmelo, Jürgen V. Vogt, Bernard Bisselink, and Ad De Roo. 2017. "Comparing soil moisture anomalies from multiple independent sources over different regions across the globe." *Hydrology and Earth System Sciences* 21: 6329–6343. https://doi.org/10.5194/hess-21-6329-2017.

Chang, Qianyu. 2020. "Mapping shrub biomass, Leaf Area Index and rainfall interception capacities in the Arctic tundra using L-band SAR." PhD diss., University of Guelph.

Climate Centre. 2024. *Climate fact sheet 2024: Mozambique*. Technical Report. Red Cross Red Crescent Climate Centre. https://www.climatecentre.org/publications/14126/mozambique/.

Dewitte, Olivier, Arwyn Jones, Otto Spaargaren, Henrik Breuning-Madsen, Michel Brossard, Almami Dampha, Jozef Deckers, et al. 2013. "Harmonisation of the soil map of Africa at the continental scale." *Geoderma* 211-212: 138–153. https://doi.org/10.1016/j.geoderma.2013.07.007.

Domingo, F., G. Sánchez, M.J. Moro, A.J. Brenner, and J. Puigdefábregas. 1998. "Measurement and modelling of rainfall interception by three semi-arid canopies." *Agricultural and Forest Meteorology* 91: 275–292. https://doi.org/https://doi.org/10.1016/S0168-1923(98)00068-9.

European Commission's Directorate-General for European Civil Protection and Humanitarian Aid Operations. 2024. *Madagascar - Tropical Cyclone ALVARO (GDACS, BNGRC, Meteo Madagascar) (ECHO Daily Flash of 3 January 2024)*. Technical Report. European Commission's Directorate-General for European Civil Protection and Humanitarian Aid Operations. https://reliefweb.int/report/madagascar/madagascar-tropical-cyclone-alvaro-gdacs-bngrc-meteo-madagascar-echo-daily-flash-3-january-2024.

Famine Early Warning Systems Network. 2020a. *Mozambique Food Security Outlook: February to September 2020*. Technical Report. Famine Early Warning Systems Network. https://fews.net/sites/default/files/documents/reports/MOZAMBIQUE_Food_Security_Outlook_02.2020_FINAL_EN.pdf.

Famine Early Warning Systems Network. 2020b. *Mozambique Food Security Outlook: June 2020 to January 2021*. Technical Report. Famine Early Warning Systems Network. https://fews.net/southern-africa/mozambique/food-security-outlook/june-2020.

Famine Early Warning Systems Network. 2024. *Mozambique Key Message Update August 2024: Food assistance needs likely to increase during upcoming lean season*. Technical Report. Famine Early Warning Systems Network. https://fews.net/southern-africa/mozambique/key-message-update/august-2024.

Famine Early Warning Systems Network. 2025. *Mozambique: Monthly Climate and Weather*. Technical Report. Famine Early Warning Systems Network and National Oceanic and Atmospheric Administration Climate Prediction Center. https://www.cpc.ncep.noaa.gov/products/international/FEWS_REPORT/Mozambique/FEWSNET_Mozambique_October2025.pdf.

Food and Agriculture Organization of the United Nations. 2021. *Mozambique: Agricultural livelihoods and food security in the context of COVID-19*. Technical Report. Food and Agriculture Organization of the United Nations. https://openknowledge.fao.org/items/316033bd-182c-4f3c-9613-1c5018deb647.

Frison, Pierre Louis, Bénédicte Fruneau, Syrine Kmiha, Kamel Soudani, Eric Dufrêne, Thuy Le Toan, Thierry Koleck, Ludovic Villard, Eric Mougin, and Jean Paul Rudant. 2018. "Potential of Sentinel-1 data for monitoring temperate mixed forest phenology." *Remote Sensing* 10: 1–10. https://doi.org/10.3390/rs10122049.

Funk, Chris, Pete Peterson, Martin Landsfeld, Diego Pedreros, James Verdin, Shraddhanand Shukla, Gregory Husak, et al. 2015. "The climate hazards infrared precipitation with stations - A new environmental record for monitoring extremes." *Scientific Data* 2. https://doi.org/10.1038/sdata.2015.66.

Gidey, Eskinder, Oagile Dikinya, Reuben Sebego, Eagilwe Segosebe, and Amanuel Zenebe. 2018. "Analysis of the long-term agricultural drought onset, cessation, duration, frequency, severity and spatial extent using Vegetation Health Index (VHI) in Raya and its environs, Northern Ethiopia." *Environmental Systems Research* 7. https://doi.org/10.1186/s40068-018-0115-z.

Global Information and Early Warning System on Food and Agriculture. 2025. *GIEWS Country Brief: The Republic of Mozambique*. Technical Report. Food and Agriculture Organization of the United Nations. https://reliefweb.int/report/mozambique/giews-country-brief-mozambique-06-october-2025.

Hahn, S., T. Melzer, and W. Wagner. 2026. "Next-generation Metop ASCAT Surface Soil Moisture datasets." *Earth System Science Data Discussions* 2026: 1–43. https://doi.org/10.5194/essd-2025-746.

Holtgrave, Ann Kathrin, Norbert Röder, Andrea Ackermann, Stefan Erasmi, and Birgit Kleinschmit. 2020. "Comparing Sentinel-1 and -2 data and indices for agricultural land use monitoring." *Remote Sensing* 12. https://doi.org/10.3390/RS12182919.

Hussain, Azfar, Ishtiaq Hussain, Shaukat Ali, Waheed Ullah, Firdos Khan, Abolfazl Rezaei, Safi Ullah, et al. 2023. "Assessment of precipitation extremes and their association with NDVI, monsoon and oceanic indices over Pakistan." *Atmospheric Research* 292. https://doi.org/10.1016/j.atmosres.2023.106873.

Ibrahim, Yahaya Z., Heiko Balzter, Jörg Kaduk, and Compton J. Tucker. 2015. "Land degradation assessment using residual trend analysis of GIMMS NDVI3g, soil moisture and rainfall in Sub-Saharan

West Africa from 1982 to 2012." *Remote Sensing* 7: 5471–5494. https://doi.org/10.3390/rs70505471.

International Center for Tropical Agriculture, and World Bank. 2017. *Climate-Smart Agriculture in Mozambique. CSA Country Profiles for Africa Series*. Technical Report. Washington, DC: International Center for Tropical Agriculture (CIAT) and World Bank. `https://climateknowledgeportal.worldbank.org/sites/default/files/2019-06/CSA-in-Mozambique.pdf`.

Ji, Lei, and Albert J. Peters. 2003. "Assessing vegetation response to drought in the northern Great Plains using vegetation and drought indices." *Remote Sensing of Environment* 87: 85–98. https://doi.org/10.1016/S0034-4257(03)00174-3.

Jiang, Rui, Arturo Sanchez-Azofeifa, Kati Laakso, Yan Xu, Zhiyan Zhou, Xiwen Luo, Junhao Huang, Xin Chen, and Yu Zang. 2021. "Cloud cover throughout all the paddy rice fields in Guangdong, China: Impacts on Sentinel 2 MSI and Landsat 8 OLI optical observations." *Remote Sensing* 13. https://doi.org/10.3390/rs13152961.

Khabbazan, Saeed, Paul Vermunt, Susan Steele-Dunne, Lexy Ratering Arntz, Caterina Marinetti, Dirk van der Valk, Lorenzo Iannini, Ramses Molijn, Kees Westerdijk, and Corné van der Sande. 2019. "Crop monitoring using Sentinel-1 data: A case study from The Netherlands." *Remote Sensing* 11. https://doi.org/10.3390/rs11161887.

Liu, Leizhen, Xi Yang, Hongkui Zhou, Shasha Liu, Lei Zhou, Xiaohan Li, Jianhua Yang, Xinyi Han, and Jianjun Wu. 2018. "Evaluating the utility of solar-induced chlorophyll fluorescence for drought monitoring by comparison with NDVI derived from wheat canopy." *Science of the Total Environment* 625: 1208–1217. https://doi.org/10.1016/j.scitotenv.2017.12.268.

Ma, Yuyang, Gongxin Jiang, Jianxi Huang, Yonglin Shen, Haixiang Guan, Yi Dong, Jialin Li, and Chuli Hu. 2024. "Evaluating the Ability of the Sentinel-1 Cross-Polarization Ratio to Detect Spring Maize Phenology Using Adaptive Dynamic Threshold." *Remote Sensing* 16. https://doi.org/10.3390/rs16050826.

Maselli, Fabio. 2004. "Monitoring forest conditions in a protected Mediterranean coastal area by the analysis of multiyear NDVI data." *Remote Sensing of Environment* 89: 423–433. https://doi.org/10.1016/j.rse.2003.10.020.

Massart, Samuel, Mariette Vreugdenhil, Rafael Rogério Borguete, Carina Villegas-Lituma, Pavan Muguda Sanjeevamurthy, Sebastian Hahn, and Wolfgang Wagner. 2025. "High-resolution drought monitoring with Sentinel-1 and ASCAT: A case-study over Mozambique." *Agricultural Water Management* 318. https://doi.org/10.1016/j.agwat.2025.109638.

Meroni, Michele, Raphaël d'Andrimont, Anton Vrieling, Dominique Fasbender, Guido Lemoine, Felix Rembold, Lorenzo Seguini, and Astrid Verhegghen. 2021. "Comparing land surface phenology of major European crops as derived from SAR and multispectral data of Sentinel-1 and -2." *Remote Sensing of Environment* 253. https://doi.org/10.1016/j.rse.2020.112232.

Moses, Oliver, O. L. Kupika, W. L. Hambira, and M. Gondwe. 2025. "A comparison of the 2023/24 El Niño with other El Niño events during 1981–2024 over the Okavango River Basin, southern Africa." *Theoretical and Applied Climatology* 156. https://doi.org/10.1007/s00704-025-05593-x.

Nairn, H. Mc, and B. Brisco. 2004. "The application of C-band polarimetric SAR for agriculture: A review." *Canadian Journal of Remote Sensing* 30: 525–542. https://doi.org/10.5589/m03-069.

Navalgund, Ranganath R, V Jayaraman, and P S Roy. 2007. "Remote sensing applications: An overview." *Current Science* 93: 1747–1766. `https://www.jstor.org/stable/24102069`.

Palmer, Wayne C. 1965. "Meteorological Drought." *U.S. Department of Commerce Weather Bureau* 30.

Richard, Y., and I. Poccard. 1998. "A statistical study of NDVI sensitivity to seasonal and interannual rainfall variations in Southern Africa." *International Journal of Remote Sensing* 19: 2907–2920. https://doi.org/10.1080/014311698214343.

Sazib, Nazmus, Iliana E. Mladenova, and John D. Bolten. 2020. "Assessing the Impact of ENSO on Agriculture Over Africa Using Earth Observation Data." *Frontiers in Sustainable Food Systems* 4. https://doi.org/10.3389/fsufs.2020.509914.

Senay, G.B., N.M. Velpuri, S. Bohms, M. Budde, C. Young, J. Rowland, and J.P. Verdin. 2015. "Chapter 9 - Drought Monitoring and Assessment: Remote Sensing and Modeling Approaches for the Famine Early Warning Systems Network." In *Hydro-Meteorological Hazards, Risks and Disasters*, edited by John F. Shroder, Paolo Paron, and Giuliano Di Baldassarre, 233–262. Boston: Elsevier.

Shorachi, Maurice, Vineet Kumar, and Susan C. Steele-Dunne. 2022. "Sentinel-1 SAR Backscatter Response to Agricultural Drought in The Netherlands." *Remote Sensing* 14. https://doi.org/10.3390/rs14102435.

Silici, Laura, Calisto Bias, and Eunice Cavane. 2015. *Sustainable agriculture for small-scale farmers in Mozambique: A scoping report*. Technical Report. IIED Country Report. `http://pubs.iied.org/14`

654IIED.

Solgi, Shahin, Seyed Hamid Ahmadi, and Sabine Julia Seidel. 2023. "Remote sensing of canopy water status of the irrigated winter wheat fields and the paired anomaly analyses on the spectral vegetation indices and grain yields." *Agricultural Water Management* 280. https://doi.org/10.1016/j.agwat.2023.108226.

Steele-Dunne, Susan C., Heather McNairn, Alejandro Monsivais-Huertero, Jasmeet Judge, Pang Wei Liu, and Kostas Papathanassiou. 2017. "Radar Remote Sensing of Agricultural Canopies: A Review." *IEEE Journal of Selected Topics in Applied Earth Observations and Remote Sensing* 10: 2249–2273. https://doi.org/10.1109/JSTARS.2016.2639043.

Sun, Linjian, Ye Zhang, Xuling Chang, Yanjie Wang, and Jiajia Xu. 2020. "Cloud-Aware Generative Network: Removing Cloud from Optical Remote Sensing Images." *IEEE Geoscience and Remote Sensing Letters* 17: 691–695. https://doi.org/10.1109/LGRS.2019.2928840.

Tadross, Mark. 2009. *Climate change modelling and analyses for Mozambique*. Technical Report. Instituto Nacional de Gestão de Calamidades. https://weadapt.org/wp-content/uploads/2023/05/5099348f543eaclimate-modelling-final-mozambique-.pdf.

Toté, Carolien, Domingos Patricio, Hendrik Boogaard, Raymond van der Wijngaart, Elena Tarnavsky, and Chris Funk. 2015. "Evaluation of satellite rainfall estimates for drought and flood monitoring in Mozambique." *Remote Sensing* 7: 1758–1776. https://doi.org/10.3390/rs70201758.

United Nations Office for the Coordination of Humanitarian Affairs. 2024a. *Tropical Cyclone Chido - Dec 2024*. Technical Report. United Nations Office for the Coordination of Humanitarian Affairs. https://reliefweb.int/disaster/tc-2024-000224-moz.

United Nations Office for the Coordination of Humanitarian Affairs. 2024b. *Tropical Storm Filipo - Mar 2024*. Technical Report. United Nations Office for the Coordination of Humanitarian Affairs. https://reliefweb.int/disaster/tc-2024-000032-moz.

United Nations Office of the Resident Coordinator. 2016. *Mozambique: Drought Office of the Resident Coordinator, Situation Report No. 4*. Technical Report. United Nations Office of the Resident Coordinator. https://reliefweb.int/report/mozambique/mozambique-drought-office-resident-coordinator-situation-report-no-4-10-june-2016.

Urban, Marcel, Christian Berger, Tami E. Mudau, Kai Heckel, John Truckenbrodt, Victor Onyango Odipo, Izak P.J. Smit, and Christiane Schmullius. 2018. "Surface moisture and vegetation cover analysis for drought monitoring in the southern Kruger National Park using Sentinel-1, Sentinel-2, and Landsat-8." *Remote Sensing* 10. https://doi.org/10.3390/rs10091482.

Veloso, Amanda, Stéphane Mermoz, Alexandre Bouvet, Thuy Le Toan, Milena Planells, Jean François Dejoux, and Eric Ceschia. 2017. "Understanding the temporal behavior of crops using Sentinel-1 and Sentinel-2-like data for agricultural applications." *Remote Sensing of Environment* 199: 415–426. https://doi.org/10.1016/j.rse.2017.07.015.

Vreugdenhil, Mariette, Isabella Greimeister-Pfeil, Preimesberger Wolfgang, Stefania Camici, Wouter Dorigo, Markus Enenkel, Robin van der Schalie, Susan Steele-Dunne, and Wolfgang Wagner. 2022. "Microwave remote sensing for agricultural drought monitoring: Recent developments and challenges." *Frontiers in Water* 4: 1–21.

Vreugdenhil, Mariette, Claudio Navacchi, Bernhard Bauer-Marschallinger, Sebastian Hahn, Susan Steele-Dunne, Isabella Pfeil, Wouter Dorigo, and Wolfgang Wagner. 2020. "Sentinel-1 cross ratio and vegetation optical depth: A comparison over Europe." *Remote Sensing* 12: 1–19. https://doi.org/10.3390/rs12203404.

Vreugdenhil, Mariette, Wolfgang Wagner, Bernhard Bauer-Marschallinger, Isabella Pfeil, Irene Teubner, Christoph Rüdiger, and Peter Strauss. 2018. "Sensitivity of Sentinel-1 backscatter to vegetation dynamics: An Austrian case study." *Remote Sensing* 10. https://doi.org/10.3390/rs10091396.

Wagner, Wolfgang, Bernhard Bauer-Marschallinger, Claudio Navacchi, Felix Reuß, Senmao Cao, Christoph Reimer, Matthias Schramm, and Christian Briese. 2021. "A Sentinel-1 backscatter datacube for global land monitoring applications." *Remote Sensing* 13. https://doi.org/10.3390/rs13224622.

Wagner, Wolfgang, Bernhard Bauer-Marschallinger, Florian Roth, Tobias Raiger-Stachl, Christoph Reimer, Niall McCormick, Patrick Matgen, et al. 2026. "The fully-automatic Sentinel-1 Global Flood Monitoring service: Scientific challenges and future directions." *Remote Sensing of Environment* 333: 115108. https://doi.org/10.1016/j.rse.2025.115108.

Wang, J., P. M. Rich, and K. P. Price. 2003. "Temporal responses of NDVI to precipitation and temperature in the central Great Plains, USA." *International Journal of Remote Sensing* 24: 2345–2364. https://doi.org/10.1080/01431160210154812.

Wei, Yujiao, Lin Zhu, Yun Chen, Xinyu Cao, and Huilin Yu. 2022. "Spatiotemporal Variations in

Drought and Vegetation Response in Inner Mongolia from 1982 to 2019." *Remote Sensing* 14. https://doi.org/10.3390/rs14153803.

West, Harry, Nevil Quinn, and Michael Horswell. 2019. "Remote sensing for drought monitoring & impact assessment: Progress, past challenges and future opportunities." *Remote Sensing of Environment* 232. https://doi.org/10.1016/j.rse.2019.111291.

World Bank. 2011. *Climate Risk and Adaptation Country Profile Mozambique*. Technical Report. World Bank Group. https://www.gfdrr.org/en/publication/climate-risk-and-adaptation-country-profile-mozambique.

World Bank. 2024. *Mozambique Agriculture Support Policy Review*. Technical Report. World Bank. https://documents1.worldbank.org/curated/en/099824507112441138/pdf/IDU1dc5095dd19c1214a7e1a4831258f79638022.pdf.

Yu, Huinan, Yajie Yang, Changjing Wang, Rui Chen, Qiaoyun Xie, Guoxiang Liu, and Gaofei Yin. 2023. "Extracting Deciduous Forests Spring Phenology From Sentinel-1 Cross Ratio Index." *IEEE Journal of Selected Topics in Applied Earth Observations and Remote Sensing* 16: 2841–2850. https://doi.org/10.1109/JSTARS.2023.3247833.

Zhang, Ruqing, Wei Shangguan, Jiajin Liu, Wenzong Dong, and Daoyuan Wu. 2024. "Assessing meteorological and agricultural drought characteristics and drought propagation in Guangdong, China." *Journal of Hydrology: Regional Studies* 51. https://doi.org/10.1016/j.ejrh.2023.101611.

Zhang, Xuan, Zengchao Hao, Vijay P. Singh, Yu Zhang, Sifang Feng, Yang Xu, and Fanghua Hao. 2022. "Drought propagation under global warming: Characteristics, approaches, processes, and controlling factors." *Science of the Total Environment* 838. https://doi.org/10.1016/j.scitotenv.2022.156021.

Zheng, Guoqiang, Tianle Zhao, and Yaohui Liu. 2024. "Cloud Removal in the Tibetan Plateau Region Based on Self-Attention and Local-Attention Models." *Sensors* 24. https://doi.org/10.3390/s24237848.

Zwieback, Simon, Qianyu Chang, Philip Marsh, and Aaron Berg. 2019. "Shrub tundra ecohydrology: Rainfall interception is a major component of the water balance." *Environmental Research Letters* 14. https://doi.org/10.1088/1748-9326/ab1049.